frontiers

Depth dependent three-layer model for the surface second-harmonic generation yield

Sean M. Anderson [1,*], **Bernardo S. Mendoza** [1]

[1] *Centro de Investigaciones en Óptica, A.C., León, Mexico*

Correspondence*:
Sean M. Anderson
Centro de Investigaciones en Óptica, A.C., Loma del Bosque 115, León, 37150, Mexico
sma@cio.mx

ABSTRACT

We present a generalization of a three-layer model to calculate the surface second harmonic generation (SSGH) yield, that includes the depth dependence of the surface nonlinear second order susceptibility tensor $\boldsymbol{\chi}(-2\omega;\omega,\omega)$. This model considers that the surface is represented by three regions or layers. The first layer is the vacuum region with a dielectric function $\epsilon_v(\omega)=1$ from where the fundamental electric field impinges on the material. The second layer is a thin layer (ℓ) of thickness d characterized by a dielectric function $\epsilon_\ell(\omega)$, and it is in this layer where the SSHG takes place. We consider the position of $\boldsymbol{\chi}(-2\omega;\omega,\omega)$ within this surface layer. The third layer is the bulk region denoted by b and characterized by $\epsilon_b(\omega)$. Both the vacuum and bulk layers are semi-infinite. The model includes the multiple reflections of both the fundamental and the second-harmonic (SH) fields that take place at the thin layer ℓ. We use the depth dependent three-layer model and compare it against the experimental results of a Si(111)(1$\times$1):H surface.

Keywords: surface, second harmonic generation, SHG, multiple, reflections, semiconductor, spectroscopy

1 INTRODUCTION

Surface second-harmonic generation (SSHG) has been shown to be an effective, nondestructive and noninvasive probe to study surface and interface properties (Chen et al., 1981; Shen, 1989; McGilp et al., 1994; Bloembergen, 1999; McGilp, 1999; Lüpke, 1999; Downer et al., 2001a,b). SSHG spectroscopy is now very cost-effective and popular because it is an efficient method for characterizing the properties of buried interfaces and nanostructures. The high surface sensitivity of SSHG spectroscopy is due to the fact that within the dipole approximation, the bulk second-harmonic generation (SHG) in centrosymmetric materials is identically zero. The SHG process can occur only at the surface where the inversion symmetry is broken. SSHG has useful applications for studying thick thermal oxides on semiconductor surfaces (Hasselt et al., 1995; Kolthammer et al., 2005) and thin films (Yeganeh et al., 1992). The accurate determination of these studies is highly dependent on multiple reflections of both the SH and fundamental waves in the surface region. These considerations have been taken into account to study thin films (Hase et al., 1992; Buinitskaya et al., 2002, 2003) and, using the Maker fringe technique (Maker et al., 1962), other materials (Tellier and Boisrobert, 2007; Abe et al., 2008).

Bloembergen and Pershan (1962) were the first to consider multiple reflections in their treatment of SHG in a nonlinear slab. However, they only considered the second-harmonic (SH) fields and derived results for a dielectric with a small linear reflectance. They also neglected the multiple reflections of the fundamental waves inside the media. Surface effects were modeled by taking the limit of a thin slab with a thickness much smaller than the wavelength of the incoming light. Ref. (Dick et al., 1985) used this methodology to determine the components of the nonlinear optical susceptibility tensor, $\boldsymbol{\chi}(-2\omega;\omega,\omega)$, of a fluorescent dye over fused silica. Later works (Sipe et al., 1987; Mizrahi and Sipe, 1988) developed a simplified method using phenomenological models in which the surface is treated as an infinitesimally thin dipole sheet. The inclusion of multiple reflections is necessary for both the SH radiation and the incoming fundamental fields; this was experimentally verified in Ref. (Morita et al., 1988), where they show that the lineshape of the SSHG radiation is composed of resonances from both the SH and fundamental waves.

As mentioned above, SSHG is particularly useful for studying the surfaces of centrosymmetric materials. From the theoretical point of view, the calculation of $\boldsymbol{\chi}(-2\omega;\omega,\omega)$ proceeds as follows. To mimic the semi-infinite system, we construct a supercell consisting of a finite slab of material plus a vacuum region. Both the size of the slab and the vacuum region should be such that the value of $\boldsymbol{\chi}(-2\omega;\omega,\omega)$ is well converged. A cut function is used to decouple the two halves of the supercell in order to obtain the value of $\boldsymbol{\chi}(-2\omega;\omega,\omega)$ for either half. If the supercell itself is centrosymmetric, the value $\boldsymbol{\chi}(-2\omega;\omega,\omega)$ for the full supercell is identically zero. Therefore, the cut function is of paramount importance in order to obtain a finite value for $\boldsymbol{\chi}(-2\omega;\omega,\omega)$ for either side of the slab (Reining et al., 1994; Anderson et al., 2015, 2016). The cut function can be generalized to one that is capable of obtaining the value of $\boldsymbol{\chi}(-2\omega;\omega,\omega)$ for any part of the slab. We can easily obtain the depth within the slab for which $\boldsymbol{\chi}(-2\omega;\omega,\omega)$ is nonzero; conversely, we can verify that it goes to zero towards the middle of the slab, where the centrosymmetry of the material is restored (Mejía et al., 2004). Therefore, for the surface of any centrosymmetric material, we can find the thickness of the layer where $\boldsymbol{\chi}(-2\omega;\omega,\omega)$ is finite.

Based on this approach for the calculation of $\boldsymbol{\chi}(-2\omega;\omega,\omega)$, in this paper we generalize the "three-layer model" for the SH radiation from the surface of a centrosymmetric material (Anderson and Mendoza, 2016). This model considers that the SH conversion takes place in a thin layer just below the surface of the material that lies under the vacuum region and above the bulk of the material. It is the three-layer model that allows us to integrate the effects of multiple reflections for both the SH and fundamental fields into the SSHG yield. As we show in this article, this treatment can be generalized to take into account the *depth* dependence of $\boldsymbol{\chi}(-2\omega;\omega,\omega)$ perpendicular to the surface. As shown in Anderson and Mendoza (2016), the inclusion of these effects is necessary to accurately model the SSHG radiation.

We develop the generalization of the model and derive expressions for the SH radiation for the commonly used polarization combinations of incoming and outgoing electric fields. We particularize these expressions for the (111) crystalline surface of a centrosymmetric material, although they could be easily applied to any surface regardless of symmetry. As an example, we present results for the SSHG yield of the Si(111)(1$\times$1):H surface and compare with the experimental results from Mejía et al. (2002). We show that the three layer model, with the multiple reflections and the depth dependence of $\boldsymbol{\chi}(-2\omega;\omega,\omega)$, improves the similarity between the theoretical and experimental spectra. We note that our treatment is strictly valid within the dipole approximation, and we assume that the bulk quadrupolar SHG response is negligible compared to the dipolar contribution, as reported in the experimental works of Refs. (Aktsipetrov et al., 1986; Sipe et al., 1987; Xu et al., 1997; Guyot-Sionnest and Shen, 1988; Downer et al., 2001b; Shen, 1999).

This paper is organized as follows. In Sec. 2, we present the relevant equations and theory that describe the SSHG yield that includes the depth dependence of $\boldsymbol{\chi}(-2\omega;\omega,\omega)$. We present our calculated results against the experimental data for the Si(111)(1×1):H surface in Sec. 3, and finally, we list our conclusions and final remarks in Sec. 4.

2 THE THREE LAYER MODEL FOR THE SSHG YIELD

In this section we generalize the results from Anderson and Mendoza (2016) in order to allow for the depth dependence of $\boldsymbol{\chi}(-2\omega;\omega,\omega)$. We first derive the formulas required for the calculation of the SSHG yield, defined by

$$\mathcal{R}(\omega)=\frac{I(2\omega)}{I^2(\omega)}, \tag{1}$$

with the intensity given by (Boyd, 2003; Sutherland, 2003)

$$I(\omega)=2\epsilon_0 c\, n(\omega)|E(\omega)|^2, \tag{2}$$

where $n(\omega)=(\epsilon(\omega))^{1/2}$ is the index of refraction, $\epsilon(\omega)$ is the dielectric function, ϵ_0 is the vacuum permittivity, and c is the speed of light in the vacuum.

The three-layer model proposed in Anderson and Mendoza (2016) considers that the surface is represented by three regions or layers. The first layer is the vacuum region (denoted by v) with a dielectric function $\epsilon_v(\omega)=1$, from where the fundamental electric field $\mathbf{E}_v(\omega)$ impinges on the material. The second layer is a thin layer (denoted by ℓ) of thickness d characterized by a dielectric function $\epsilon_\ell(\omega)$; it is in this layer where the SHG process takes place. The third layer is the bulk region denoted by b and characterized by $\epsilon_b(\omega)$. Both the vacuum and bulk layers are semi-infinite (see Fig. 1).

The electromagnetic response of the three-layer model proposed in Anderson and Mendoza (2016) is generalized as follows,

$$\mathbf{P}_\ell(\mathbf{r},t)=\boldsymbol{\mathcal{P}}_\ell(z)e^{i\hat{\boldsymbol{\kappa}}\cdot\mathbf{R}}e^{-i\omega t}+\text{c.c.}, \tag{3}$$

where $\boldsymbol{\mathcal{P}}_{\boldsymbol{\ell}}(z)$ is the now depth dependent polarization, that was previously considered to be constant throughout the layer ℓ (Anderson and Mendoza, 2016). In this equation, $\mathbf{R}=(x,y)$, where x,y,z are the Cartesian directions and $\hat{\mathbf{x}}$, $\hat{\mathbf{y}}$, $\hat{\mathbf{z}}$ their unit vectors, respectively, with z being positive in the vacuum region and xy defining the surface plane. We have that $\hat{\boldsymbol{\kappa}}=\cos\phi\hat{\mathbf{x}}+\sin\phi\hat{\mathbf{y}}$ is the component of the wave vector $\boldsymbol{\nu}_\ell$ parallel to the surface, and ϕ is the azimuthal angle that the plane of incidence makes with $\hat{\mathbf{x}}$. The nonlinear polarization responsible for the SHG is immersed in the thin layer ℓ, and is given by

$$\mathcal{P}_\ell^{\mathrm{a}}(z;2\omega)=\epsilon_0\chi^{\mathrm{abc}}(z;-2\omega;\omega,\omega)E_\ell^{\mathrm{b}}(z;\omega)E_\ell^{\mathrm{c}}(z;\omega) \tag{4}$$

where $\boldsymbol{\chi}(z;-2\omega;\omega,\omega)$ is the dipolar surface nonlinear depth-dependent susceptibility tensor, and the Cartesian superscripts (a, b, and c) are summed over if repeated. For ease of notation we simply use $\boldsymbol{\chi}(z)$. Also, $\chi^{\mathrm{abc}}(z)=\chi^{\mathrm{acb}}(z)$ due to the intrinsic permutation symmetry, since SHG is degenerate in $E_\ell^{\mathrm{b}}(z;\omega)$ and $E_\ell^{\mathrm{c}}(z;\omega)$.

To continue, we first approximate the linear field $\mathbf{E}(z;\omega)$ as independent of the z position. The calculation of position dependence of the linear field is a complicated problem worth pursuing, but is outside the scope of this work. Therefore, the first approximation of the depth dependence of $\mathbf{E}(z,\omega)$ is accounted for by the inclusion of the Fresnel factors as given in Anderson and Mendoza (2016). Indeed, $\mathbf{E}_\ell(z,\omega)=E_0\mathbf{e}_\ell^{\mathrm{i}}$, where E_0 is the intensity of the fundamental field, and $\mathbf{e}^{\mathrm{i}}$ is a "Fresnel vector" for $\mathrm{i}=s$ or $\mathrm{i}=p$ polarization of the incoming field $\mathrm{E}_v(\omega)$ given by

$$\mathbf{e}_\ell^{\omega,s} = t_s^{v\ell} r_s^{M+}\hat{\mathbf{s}}, \tag{5}$$

where $\hat{\mathbf{s}} = \hat{\boldsymbol{\kappa}} \times \hat{\mathbf{z}}$ is the unit vector for s polarization, and

$$\mathbf{e}_\ell^{\omega,p} = \frac{t_p^{v\ell}}{n_\ell}\left(r_p^{M+}\sin\theta_0\hat{\mathbf{z}} + r_p^{M-} w_\ell \hat{\boldsymbol{\kappa}}\right). \tag{6}$$

We define the linear reflection coefficient r_i^M as

$$r_\mathrm{i}^M \equiv \frac{r_\mathrm{i}^{\ell b} e^{i\varphi}}{1 + r_\mathrm{i}^{v\ell} r_\mathrm{i}^{\ell b} e^{i\varphi}}, \quad \mathrm{i} = s, p, \tag{7}$$

and

$$r_\mathrm{i}^{M\pm} = 1 \pm r_\mathrm{i}^M, \quad \mathrm{i} = s, p. \tag{8}$$

This coefficient accounts for the multiple (M) reflections of the fundamental field, that depends on the thickness d of the layer ℓ included in the phase $\varphi = 4\pi(d/\lambda_0)w_\ell(\omega)$, where λ_0 is the wavelength of the incoming light, $w_\ell(\omega) = (\epsilon_\ell(\omega) - \sin^2\theta_0)^{1/2}$, θ_0 is the angle of incidence, and $n_\ell = (\epsilon_\ell(\omega))^{1/2}$. The Fresnel factors, t_i^{ij} and r_i^{ij} for the vacuum-layer ($ij = v\ell$) and layer-bulk ($ij = \ell b$) interfaces, are given by the standard formulas (Jackson, 1998),

$$\begin{aligned}
t_s^{ij}(\omega) &= \frac{2w_i(\omega)}{w_i(\omega) + w_j(\omega)},\\
t_p^{ij}(\omega) &= \frac{2w_i(\omega)\sqrt{\epsilon_i(\omega)\epsilon_j(\omega)}}{w_i(\omega)\epsilon_j(\omega) + w_j(\omega)\epsilon_i(\omega)},\\
r_s^{ij}(\omega) &= \frac{w_i(\omega) - w_j(\omega)}{w_i(\omega) + w_j(\omega)},\\
r_p^{ij}(\omega) &= \frac{w_i(\omega)\epsilon_j(\omega) - w_j\epsilon_i(\omega)}{w_i(\omega)\epsilon_j(\omega) + w_j(\omega)\epsilon_i(\omega)},
\end{aligned} \tag{9}$$

where $w_i(\omega) = (\epsilon_i(\omega) - \sin^2\theta_0)^{1/2}$ for $i = \ell, b$, or v. The Fresnel factors in uppercase letters, $T_{s,p}^{ij}$ and $R_{s,p}^{ij}$, are evaluated at 2ω from their corresponding lower case counterparts given above, i.e. $T_{s,p}^{ij} = t_{s,p}^{ij}(2\omega)$ and $R_{s,p}^{ij} = r_{s,p}^{ij}(2\omega)$. These factors will appear in the following sections.

2.1 Depth-dependance

The calculation of $\boldsymbol{\chi}(z)$ using the layer-by-layer method has been developed in detail in Anderson et al. (2015). Indeed, we calculate $\boldsymbol{\chi}(z_n)$ at fixed positions z_n, where $n = 1, 2, 3, \ldots, N/2$ denotes the atomic layer within the slab and N is the total number of atomic layers used in the supercell method, as described in the introduction. We take $n = 1$ as the top-most atomic layer and $n = N/2$ as the middle atomic layer, where it is expected that $\boldsymbol{\chi}(z_{N/2}) = 0$ due to the centrosymmetric environment at the center of the supercell (Anderson et al., 2015). To obtain the SH radiated field induced by the nonlinear polarization of Eq. (4), we generalize Eq. (35) from Anderson and Mendoza (2016) as

$$E_\ell(z_n; 2\omega) = \frac{i\omega}{c\cos\theta_0}\mathbf{e}_\ell^{2\omega,\mathrm{F}}(z_n) \cdot \boldsymbol{\chi}(z_n) : \mathbf{e}_\ell^{\omega,\mathrm{i}}\mathbf{e}_\ell^{\omega,\mathrm{i}}, \tag{10}$$

which is the nonlinear field radiated from depth z_n as induced by $\boldsymbol{\chi}(z_n)$. In this expression, i=s, p denotes the incoming polarization of the incident field, where $\mathbf{e}_\ell^{\omega,\mathrm{i}}$ are given by Eqs. (5) and (6). Eqs. (40) and (41) from Anderson and Mendoza (2016) are also generalized to obtain the following results for $\mathbf{e}_\ell^{2\omega,\mathrm{F}}(z_n)$,

$$\mathbf{e}_\ell^{2\omega,P}(z_n) = \frac{T_p^{v\ell}}{N_\ell}\big(\sin\theta_0 R_p^{M+}(z_n)\hat{\mathbf{z}} - W_\ell R_p^{M-}(z_n)\cos\phi\hat{\mathbf{x}} - W_\ell R_p^{M-}(z_n)\sin\phi\hat{\mathbf{y}}\big), \tag{11}$$

for F$= P$ outgoing polarization, and

$$\mathbf{e}_\ell^{2\omega,S} = T_s^{v\ell} R_s^{M+}(z_n)\left(-\sin\phi\hat{\mathbf{x}} + \cos\phi\hat{\mathbf{y}}\right). \tag{12}$$

for F$= S$ outgoing polarization. Here,

$$R_\mathrm{i}^{M\pm}(z_n) = 1 \pm R_\mathrm{i}^{M}(z_n), \tag{13}$$

and

$$R_\mathrm{i}^{M}(z_n) \equiv \frac{R_\mathrm{i}^{\ell b}}{1 + R_\mathrm{i}^{v\ell} R_\mathrm{i}^{\ell b} e^{i\delta}} e^{i8\pi W_\ell (z_n/\lambda_0)}, \quad \mathrm{i} = s, p, \tag{14}$$

is the reflection coefficient that takes into account the multiple reflections of the SH field within the layer ℓ. $W_\ell = (\epsilon_\ell(2\omega) - \sin^2\theta_0)^{1/2}$, $N_\ell = (\epsilon_\ell(2\omega))^{1/2}$, $\delta = 8\pi(d/\lambda_0)W_\ell$, and the Fresnel factors T_i^{ij} and R_i^{ij} are given in Eq. (9).

Considering the above, we calculate the total radiated SH field as

$$\begin{aligned} E_\ell(2\omega) &= \frac{1}{N/2}\sum_{n=1}^{N/2} E_\ell(z_n;2\omega) \\ &= \frac{i\omega}{c\cos\theta_0}\frac{1}{N/2}\sum_{n=1}^{N/2} \mathbf{e}_\ell^{2\omega,\mathrm{F}}(z_n)\cdot\boldsymbol{\chi}(z_n) : \mathbf{e}_\ell^{\omega,\mathrm{i}}\mathbf{e}_\ell^{\omega,\mathrm{i}} \\ &= \frac{i\omega}{c\cos\theta_0}\frac{1}{N/2}\sum_{n=1}^{N/2} \Upsilon_{\mathrm{iF}}(z_n), \end{aligned} \tag{15}$$

where

$$\Upsilon_{\mathrm{iF}}(z_n) = \mathbf{e}_\ell^{2\omega,\mathrm{F}}(z_n)\cdot\boldsymbol{\chi}(z_n) : \mathbf{e}_\ell^{\omega,\mathrm{i}}\mathbf{e}_\ell^{\omega,\mathrm{i}}. \tag{16}$$

Finally, the SSHG yield (Eq. (1)) can be expressed as

$$\mathcal{R}_{\mathrm{iF}}(2\omega) = \frac{\omega^2}{2\epsilon_0 c^3\cos^2\theta_0}\left|\frac{1}{n_\ell}\frac{1}{N/2}\sum_{n=1}^{N/2}\Upsilon_{\mathrm{iF}}(z_n)\right|^2. \tag{17}$$

Note that $\boldsymbol{\chi}(z_n)$ is given in m^2/V since it is a surface second order nonlinear susceptibility, and $\mathcal{R}_{\mathrm{iF}}(2\omega)$ is in m^2/W. Lastly, we have that (Anderson and Mendoza, 2016),

$$
\begin{aligned}
\mathbf{e}_\ell^{\omega,\mathrm{p}}\mathbf{e}_\ell^{\omega,\mathrm{p}} = \left(\frac{t_p^{v\ell}}{n_\ell}\right)^2 \Big(&\left(r_p^{M-}\right)^2 w_\ell^2 \cos^2\phi\,\hat{\mathbf{x}}\hat{\mathbf{x}} + 2\left(r_p^{M-}\right)^2 w_\ell^2 \sin\phi\cos\phi\,\hat{\mathbf{x}}\hat{\mathbf{y}} \\
&+ \left(r_p^{M-}\right)^2 w_\ell^2 \sin^2\phi\,\hat{\mathbf{y}}\hat{\mathbf{y}} + 2 r_p^{M+} r_p^{M-} w_\ell \sin\theta_0 \sin\phi\,\hat{\mathbf{y}}\hat{\mathbf{z}} \\
&+ \left(r_p^{M+}\right)^2 \sin^2\theta_0\,\hat{\mathbf{z}}\hat{\mathbf{z}} + 2 r_p^{M+} r_p^{M-} w_\ell \sin\theta_0 \cos\phi\,\hat{\mathbf{x}}\hat{\mathbf{z}} \Big)
\end{aligned}
\tag{18}
$$

for i $= p$ incoming polarization, and

$$
\mathbf{e}_\ell^{\omega,\mathrm{s}}\mathbf{e}_\ell^{\omega,\mathrm{s}} = \left(t_s^{v\ell} r_s^{M+}\right)^2 \left(\sin^2\phi\hat{\mathbf{x}}\hat{\mathbf{x}} + \cos^2\phi\hat{\mathbf{y}}\hat{\mathbf{y}} - 2\sin\phi\cos\phi\hat{\mathbf{x}}\hat{\mathbf{y}}\right) \tag{19}
$$

for i $= s$ incoming polarization.

From the formulation above, we can derive the SSHG yield $\mathcal{R}_{\mathrm{iF}}$ for the usual combinations of pP, pS, sP, and sS incoming and outgoing polarizations as shown in Anderson and Mendoza (2016). To better view the effects of the z-dependence of $\boldsymbol{\chi}(z_n)$ on the SHG yield, we will apply our formulation on a test surface. We choose the Si(111)1$\times$1:H surface, since the (111) symmetry relations has only four nonzero components, and we can directly compare our theoretical calculations with experimental data available in Mejía et al. (2002). We only present results for the p-in P-out ($\mathcal{R}_{pP}$) polarization case since it has the strongest yield, and thus the best signal-to-noise ratio for the measured data.

The (111) surface has only the following nonzero components of $\boldsymbol{\chi}(z_n)$: $\chi^{zzz}(z_n)$, $\chi^{zxx}(z_n) = \chi^{zyy}(z_n)$, $\chi^{xxz}(z_n) = \chi^{yyz}(z_n)$ and $\chi^{xxx}(z_n) = -\chi^{xyy}(z_n) = -\chi^{yyx}(z_n)$, so we can easily work out that

$$
\begin{aligned}
\Upsilon_{pP}(z_n) = \frac{T_p^{v\ell}}{N_\ell}\left(\frac{t_p^{v\ell}}{n_\ell}\right)^2 \Bigg(&\sin\theta_0 \Big[\left(r_p^{M+}\right)^2 \sin^2\theta_0 R_p^{M+}(z_n)\chi^{zzz}(z_n) + \left(r_p^{M-}\right)^2 w_\ell^2 R_p^{M+}(z_n)\chi^{zxx}(z_n) \Big] \\
&- w_\ell W_\ell \Big[2 r_p^{M+} r_p^{M-} \sin\theta_0 R_p^{M-}(z_n)\chi^{xxz}(z_n) + \left(r_p^{M-}\right)^2 w_\ell R_p^{M-}(z_n)\chi^{xxx}(z_n)\cos 3\phi \Big] \Bigg),
\end{aligned}
\tag{20}
$$

where the three-fold azimuthal symmetry of the SHG signal that is typical of the C_{3v} symmetry group is seen in the 3ϕ argument of the cosine function.

3 THE SSHG YIELD OF THE SI(111)1x1:H SURFACE FOR *P*-IN, *P*-OUT POLARIZATION

We consider that the Si(111)(1$\times$1):H surface is an excellent case to test the versatility of the three layer model; in particular, to study the effect that the z dependence of $\chi^{\mathrm{abc}}(z_n)$ and the multiple reflections will have on the SSHG yield. This surface is experimentally well-characterized (Mitchell et al., 2001; Mejía et al., 2002; Bergfeld et al., 2004) and there has been success in reproducing these experimental results using the three layer model with and without multiple reflections (Anderson et al., 2016; Anderson and Mendoza, 2016). The details of the *ab initio* calculation of χ^{abc} are discussed in Anderson et al. (2016). We note that we apply a scissors shift of 0.7 eV to the theoretical spectra in order to include the effects of the electronic many-body interactions within the independent particle approach of our *ab initio* calculation. This 0.7 eV value allows the SH resonant peaks to acquire their corresponding energy positions, and is obtained from a G_0W_0 calculation (Li and Galli, 2010; Anderson et al., 2016).

The number of layers N for which χ^{abc} converges, is a compromise between accuracy and the expenditure of computational time and resources. We found that $N = 50$, which includes 2 layers of H and 48 layers of Si, is an excellent compromise. Recall that the slab used in the calculation is centrosymmetric, and that only half of the atomic layers of the slab are what actually contribute to χ^{abc}. In Fig. 2 we show $\chi^{\mathrm{xxz}}(z_n)$, which is the largest component that contributes to $\mathcal{R}_{pP}$, for several choices of z_n. z_1 is the layer that corresponds to the H layer. Then, in order to recover the centrosymmetric environment of the (111) surface we must add pairs of atomic layers so that they include a vertical bond and a slanted bond of the tetrahedral unit cell corresponding to this face. This is described in detail in Mejía et al. (2004). In this way, as we move from the surface towards the bulk of the system, χ^{xxz} goes to zero. In the same figure we show $\chi^{\mathrm{xxz}}(z_2) + \chi^{\mathrm{xxz}}(z_3)$, which correspond to the first and second Si layers, and $\chi^{\mathrm{xxz}}(z_{24}) + \chi^{\mathrm{xxz}}(z_{25})$, which correspond to the last two Si layers of the half-slab. From the figure we see that the H contribution is negligible, as expected from the fact that H saturates the dangling bond of the topmost Si, quenching the response (Mejía et al., 2002). We show that the contribution from the deepest Si layers (z_{24} and z_{25}), is small compared to the topmost layers. One would expect that the contribution of the former should be zero as they are in a centrosymmetric environment. Given the relatively small size of the slab, this calculation only gives the correct qualitative result. Note that in general, we find that

$$\sum_{n=1}^{23} \chi^{\mathrm{abc}}(z_n) >> \chi^{\mathrm{abc}}(z_{24}) + \chi^{\mathrm{abc}}(z_{25}), \tag{21}$$

and thus χ^{abc} is well converged. From these findings, we can establish that the thickness of the layer ℓ where the SHG takes place is around $d = 3.6$ nm for $N/2 = 25$ active layers of SHG. These results prompt us to propose the following plausible scenario. We could use a larger value for d in order to achieve $\chi^{\mathrm{abc}}(z_{N/2-1}) + \chi^{\mathrm{abc}}(z_{N/2}) = 0$, for which we need to go to increasingly larger slabs. But in order to keep the computational burden reasonable, we could use $N = 50$ and only change the value of z_n such that $d = \sum_n z_n$ gives the new chosen value of d. In view of Eq. (21), we can keep the same value for each of the $\chi^{\mathrm{abc}}(z_n)$ components already calculated for $N = 50$. This would be equivalent to say that from Eq. (15), we have that

$$\sum_{n=1}^{23} \Upsilon_{\mathrm{iF}}(z_n) >> \Upsilon_{\mathrm{iF}}(z_{24}) + \Upsilon_{\mathrm{iF}}(z_{25}), \tag{22}$$

regardless of the actual value of z_n. We will analyze this plausible scenario as follows.

In Fig. 3, we compare the theoretical results for the SSHG yield with the experimental results from Mejía et al. (2002). We use $\theta = 65^\circ$, $\phi = 30^\circ$ and a broadening of $\sigma = 0.075$ eV. We present $\mathcal{R}_{pP}$ compared to the experimental data. With $\phi = 30^\circ$, the contribution of χ^{xxx} from Eq. (20) is completely eliminated. First, we note that the experimental spectrum shows two very well defined resonances which come from electronic transitions from the valence to the conduction bands around the known $E_1 \sim 3.4$ eV and $E_2 \sim 4.3$ eV critical points of bulk Si (Yu and Cardona, 2005). The theoretical results reproduce the features of the spectrum, although we see that the E_2 peak is blueshifted by around 0.3 eV; details on the physics that lead to such a blueshifted theoretical spectrum are given in Anderson et al. (2016). All the curves in this figure which include multiple reflections consider the following choices. First, we present the layer-by-layer calculation for a layer thickness of $d = 3.6$ nm. This is the thickness of $N/2 = 25$ atomic layers with the different z_n positions obtained directly from the slab used in the full *ab initio* calculation. We used the scenario proposed in the previous paragraph for the $d = 10$ nm curve, where the z_n positions are now stretched by a factor of 2.7, and the same $\chi^{\rm abc}(z_n)$ of the *ab initio* calculation are used in the calculation of $\mathcal{R}_{pP}$.

We can clearly see that $\mathcal{R}_{pP}$ for the layered calculation using $d = 3.6$ nm (the value from the slab) differs from the one with the stretched values of z_n that lead to $d = 10$ nm. These enhancements are larger for E_2 than for E_1. This can be understood from the fact that the corresponding λ_0 for E_1 is larger than that of E_2. From Eqs. (7) and (14), we see that the phase shifts are larger for E_2 than for E_1, producing a larger enhancement of the SSHG yield at E_2 from the multiple reflections. As the phase shifts grow with d, so does the enhancement caused by the multiple reflections. We have also verified that the effects of the multiple reflections from the linear field are significantly smaller than those of the SH field. This is clear since the phase shift of Eq. (14) is not only a factor of 2 smaller than that of Eqs. (7), but also $w_\ell < W_\ell$. For larger energies, such as E_2, λ_0 becomes smaller and the multiple reflection effects become more noticeable. The selected value for $d << \lambda_0$, which comes naturally from the *ab initio* calculation of $\chi^{\rm abc}$, is thus very reasonable in order to model a thin surface layer below the vacuum region where the nonlinear SH conversion takes place. Moreover, choosing a larger value d improves the peak ratio E_2/E_1 from 1.8 ($d = 3.6$ nm) to 2.0 ($d = 10$ nm), which is closer to the experimental value of 2.8 (Anderson and Mendoza, 2016).

Finally, in the same figure, we used the half-slab value of $\chi^{\rm abc}$, i.e.

$$\chi^{\rm abc}_{\rm hs} = \sum_{n=1}^{N/2} \chi^{\rm abc}(z_n), \tag{23}$$

along with the average value of Eq. (14), as proposed in Anderson and Mendoza (2016),

$$\bar{R}^M_{\rm i} \equiv \frac{1}{d}\int_0^d R^M_{\rm i}(z)\,dz = \frac{R^{\ell b}_{\rm i} e^{i\delta/2}}{1 + R^{v\ell}_{\rm i} R^{\ell b}_{\rm i} e^{i\delta}} \mathrm{sinc}(\delta/2), \tag{24}$$

This choice is very similar to placing $\chi^{\rm abc}(z_n)$ at $z_n \to d/2$ in Eq. (14), which can be interpreted as placing the nonlinear polarization sheet in the middle of the thin layer ℓ. Note that the average value obtained by using $\bar{R}^M_p$ with $d = 3.6$ nm is very similar to the full result using the same $d = 3.6$ nm. In general, this means that using $\chi^{\rm abc}_{\rm hs}$ in combination with $\bar{R}^M_i$ is an good strategy to calculate the SHG yield.

4 CONCLUSIONS

We have derived a formalism to calculate the SSHG yield, based on the three layer model that describes the radiating system. This treatment includes the effects of multiple reflections inside the material from both the SH and fundamental fields, and also takes into account the depth variation of the second order nonlinear susceptibility $\chi^{\rm abc}(z_n)$. The results obtained from using the theory developed here were applied to the p-in and P-out SHG yield of a Si(111)(1×1):H surface. Our depth-dependent three-layer model reproduces key spectral features and yields an intensity very close to experiment. We consider it an upgrade over our previous model (Anderson and Mendoza, 2016). The inclusion of the depth dependence yields results that is independent of the thickness d of the layer in which the SHG takes place, and requires no other free parameters.

CONFLICT OF INTEREST STATEMENT

The authors declare that the research was conducted in the absence of any commercial or financial relationships that could be construed as a potential conflict of interest.

AUTHOR CONTRIBUTIONS

SA: literature review, programming, and calculations. BM: mathematical framework and general theory. Both: manuscript preparation.

FUNDING

This work was funded by the Consejo Nacional de Ciencia y Tecnología, México via scholarship #349278, and through partial support from grant #153930.

REFERENCES

Abe, M., Shoji, I., Suda, J., and Kondo, T. (2008). Comprehensive analysis of multiple-reflection effects on rotational Maker-fringe experiments. *J. Opt. Soc. Am. B* 25, 1616. doi:10.1364/JOSAB.25.001616

Aktsipetrov, A., Baranova, I. M., and Il'inskii, A. (1986). Surface contribution to the generation of reflected second-harmonic light for centrosymmetric semiconductors. *J. Exp. Theor. Phys.* 64, 167

Anderson, S. M. and Mendoza, B. S. (2016). Three-layer model for the surface second-harmonic generation yield including multiple reflections. *Phys. Rev. B* 94, 115314. doi:10.1103/PhysRevB.94.115314

Anderson, S. M., Tancogne-Dejean, N., Mendoza, B. S., and Véniard, V. (2016). Improved *ab initio* calculation of surface second-harmonic generation from si(111)(1×1)h. *Phys. Rev. B* 93, 235304. doi:10.1103/PhysRevB.93.235304

Anderson, S. M., Tancogne-Dejean, N., Mendoza, B. S., and Véniard, V. (2015). Theory of surface second-harmonic generation for semiconductors including effects of nonlocal operators. *Phys. Rev. B* 91, 075302. doi:10.1103/PhysRevB.91.075302

Bergfeld, S., Braunschweig, B., and Daum, W. (2004). Nonlinear Optical Spectroscopy of Suboxides at Oxidized Si(111) Interfaces. *Phys. Rev. Lett.* 93, 097402. doi:10.1103/PhysRevLett.93.097402

Bloembergen, N. (1999). Surface nonlinear optics: a historical overview. *Appl. Phys. B-Lasers O.* 68, 289–293. doi:10.1007/s003400050621

Bloembergen, N. and Pershan, P. S. (1962). Light Waves at the Boundary of Nonlinear Media. *Physical Review* 128, 606–622. doi:10.1103/PhysRev.128.606

Boyd, R. (2003). *Nonlinear Optics* (New York: Academic Press)

Buinitskaya, G., Kravetsky, I., Kulyuk, L., Mirovitskii, V., and Rusu, E. (2002). Optical Second Harmonic Generation In ZnO Film: Multiple-reflection Effects. *Moldavian Journal of the Physical Sciences* 1, 77–81

Buinitskaya, G., Kravetsky, I., Kulyuk, L., Mirovitskii, V., and Rusu, E. (2003). Characterization of thin ZnO film by optical second harmonic generation: experiment and theory. In *Semiconductor Conference, 2003. CAS 2003. International*. vol. 2, 322. doi:10.1109/SMICND.2003.1252444

Chen, C. K., de Castro, A. R. B., and Shen, Y. R. (1981). Surface-enhanced second-harmonic generation. *Phys. Rev. Lett.* 46, 145–148. doi:10.1103/PhysRevLett.46.145

Dick, B., Gierulski, A., Marowsky, G., and Reider, G. A. (1985). Determination of the nonlinear optical susceptibility $\chi^{(2)}$ of surface layers by sum and difference frequency generation in reflection and transmission. *Appl. Phys. B* 38, 107–116. doi:10.1007/BF00697449

Downer, M. C., Jiang, Y., Lim, D., Mantese, L., Wilson, P. T., Mendoza, B. S., et al. (2001a). Optical second harmonic spectroscopy of silicon surfaces, interfaces and nanocrystals. *Phys. Status Solidi A* 188, 1371–1381. doi:10.1002/1521-396X(200112)188:4⟨1371::AID-PSSA1371⟩3.0.CO;2-U

Downer, M. C., Mendoza, B. S., and Gavrilenko, V. I. (2001b). Optical second harmonic spectroscopy of semiconductor surfaces: advances in microscopic understanding. *Surf. Interface Anal.* 31, 966–986. doi:10.1002/sia.1133

Guyot-Sionnest, P. and Shen, Y. R. (1988). Bulk contribution in surface second-harmonic generation. *Phys. Rev. B* 38, 7985–7989. doi:10.1103/PhysRevB.38.7985

Hase, Y., Kumata, K., Kano, S. S., Ohashi, M., Kondo, T., Ito, R., et al. (1992). New method for determining the nonlinear optical coefficients of thin films. *Appl. Phys. Lett.* 61, 145–146. doi:10.1063/1.108199

Hasselt, C. W. v., Devillers, M. A. C., Rasing, T., and Aktsipetrov, O. A. (1995). Second-harmonic generation from thick thermal oxides on Si(111): the influence of multiple reflections. *J. Opt. Soc. Am. B* 12, 33. doi:10.1364/JOSAB.12.000033

Jackson, J. D. (1998). *Classical Electrodynamics, 3rd Edition* (Wiley-VCH), 3rd edition edn.

Kolthammer, W. S., Barnard, D., Carlson, N., Edens, A. D., Miller, N. A., and Saeta, P. N. (2005). Harmonic generation in thin films and multilayers. *Phys. Rev. B* 72, 045446. doi:10.1103/PhysRevB.72.045446

Li, Y. and Galli, G. (2010). Electronic and spectroscopic properties of the hydrogen-terminated Si(111) surface from ab initio calculations. *Phys. Rev. B* 82, 045321. doi:10.1103/PhysRevB.82.045321

Lüpke, G. (1999). Characterization of semiconductor interfaces by second-harmonic generation. *Surf. Sci. Rep.* 35, 75–161. doi:10.1016/S0167-5729(99)00007-2

Maker, P. D., Terhune, R. W., Nisenoff, M., and Savage, C. M. (1962). Effects of Dispersion and Focusing on the Production of Optical Harmonics. *Phys. Rev. Lett.* 8, 21–22. doi:10.1103/PhysRevLett.8.21

McGilp, J. F. (1999). Second-harmonic generation at semiconductor and metal surfaces. *Surf. Rev. Lett.* 6, 529–558. doi:10.1142/S0218625X99000494

McGilp, J. F., Cavanagh, M., Power, J. R., and O'Mahony, J. D. (1994). Probing semiconductor interfaces using nonlinear optical spectroscopy. *Opt. Eng.* 33, 3895–3900. doi:10.1117/12.186373

Mejía, J. E., Mendoza, B. S., Palummo, M., Onida, G., Del Sole, R., Bergfeld, S., et al. (2002). Surface second-harmonic generation from si (111)(1x1) h: Theory versus experiment. *Phys. Rev. B* 66, 195329. doi:10.1103/PhysRevB.66.195329

Mejía, J. E., Mendoza, B. S., and Salazar, C. (2004). Layer-by-layer analysis of second harmonic generation at a simple surface. *Revista Mexicana de Física* 50, 134–139

Mitchell, S. A., Mehendale, M., Villeneuve, D. M., and Boukherroub, R. (2001). Second harmonic generation spectroscopy of chemically modified Si(1 1 1) surfaces. *Surf. Sci.* 488, 367–378. doi:10.1016/S0039-6028(01)01161-X

Mizrahi, V. and Sipe, J. E. (1988). Phenomenological treatment of surface second-harmonic generation. *J. Opt. Soc. Am. B* 5, 660–667. doi:10.1364/JOSAB.5.000660

Morita, R., Kondo, T., Kaneda, Y., Sugihashi, A., Ogasawara, N., Umegaki, S., et al. (1988). Multiple-Reflection Effects in Optical Second-Harmonic Generation. *Japanese Journal of Applied Physics* 27, L1134–L1136. doi:10.1143/JJAP.27.L1134

Reining, L., Del Sole, R., Cini, M., and Ping, J. G. (1994). Microscopic calculation of second-harmonic generation at semiconductor surfaces: As/Si(111) as a test case. *Phys. Rev. B* 50, 8411–8422. doi:10.1103/PhysRevB.50.8411

Shen, Y. R. (1989). Surface properties probed by second-harmonic and sum-frequency generation. *Nature* 337, 519–525. doi:10.1038/337519a0

Shen, Y. R. (1999). Surface contribution versus bulk contribution in surface nonlinear optical spectroscopy. *Appl. Phys. B* 68, 295–300. doi:10.1007/s003400050622

Sipe, J. E., Moss, D. J., and van Driel, H. M. (1987). Phenomenological theory of optical second- and third-harmonic generation from cubic centrosymmetric crystals. *Phys. Rev. B* 35, 1129–1141. doi:10.1103/PhysRevB.35.1129

Sutherland, R. L. (2003). *Handbook of Nonlinear Optics* (CRC Press)

Tellier, G. and Boisrobert, C. (2007). Second harmonic generation: Effects of the multiple reflections of the fundamental and the second harmonic waves on the Maker fringes. *Optics Communications* 279, 183–195. doi:10.1016/j.optcom.2007.06.048

Xu, Z., Hu, X. F., Lim, D., Ekerdt, J. G., and Downer, M. C. (1997). Second harmonic spectroscopy of Si(001) surfaces: Sensitivity to surface hydrogen and doping, and applications to kinetic measurements. *J. Vac. Sci. Technol. B* 15, 1059–1064. doi:10.1116/1.589415

Yeganeh, M. S., Qi, J., Culver, J. P., Yodh, A. G., and Tamargo, M. C. (1992). Interference in reflected second-harmonic generation from thin nonlinear films. *Phys. Rev. B* 46, 1603–1610. doi:10.1103/PhysRevB.46.1603

Yu, P. and Cardona, M. (2005). *Fundamentals of Semiconductors: Physics and Materials Properties* (Springer Science & Business Media), third edn.

FIGURE CAPTIONS

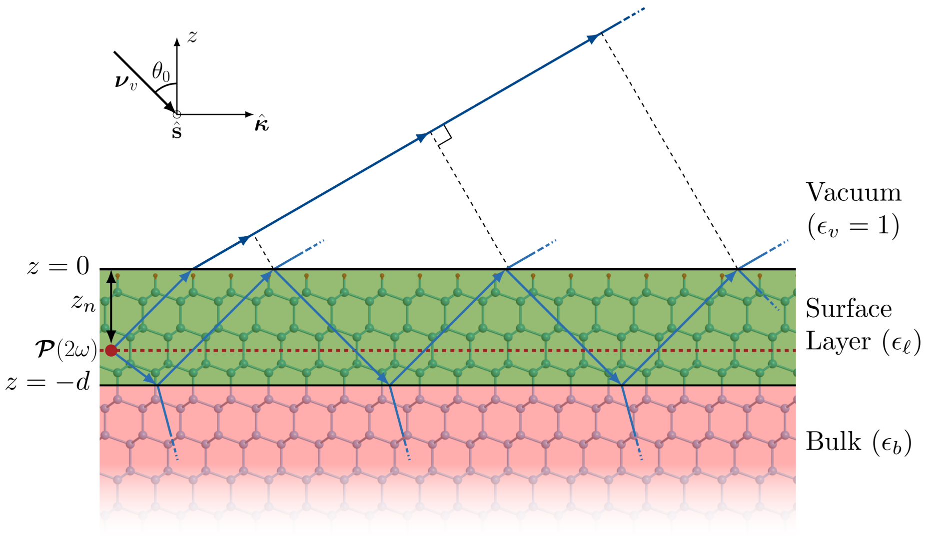

Figure 1. (Color online) Sketch of the three layer model for SHG. The vacuum region (v) is on top with $\epsilon_v = 1$; the layer ℓ of thickness d, is characterized by $\epsilon_\ell(\omega)$, and it is where the SH polarization sheet $\boldsymbol{\mathcal{P}}_\ell(2\omega)$ is located at a distance z_n. The bulk b is described by $\epsilon_b(\omega)$. The blue lines within the slab represent the SH multiple reflections. The Si(111)(1×1):H surface is represented by the ball and stick model (H: small spheres, Si: large spheres) in the background. The red dotted line is the one of the many possible z_n positions.

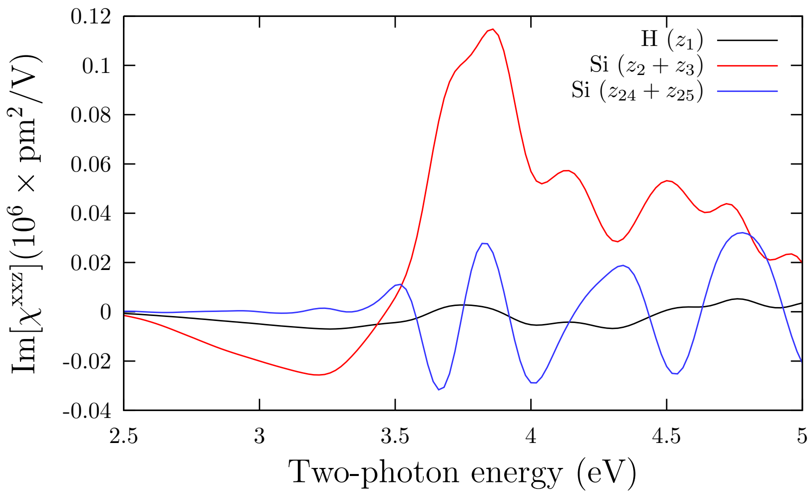

Figure 2. (Color online) Imaginary part of $\chi^{xxz}(z_n)$ for the H layer (z_1), the sum of the two topmost Si layers ($z_2 + z_3$), and the sum of the bottommost Si layers ($z_{24} + z_{25}$) for the 25 layer half-slab used in this work.

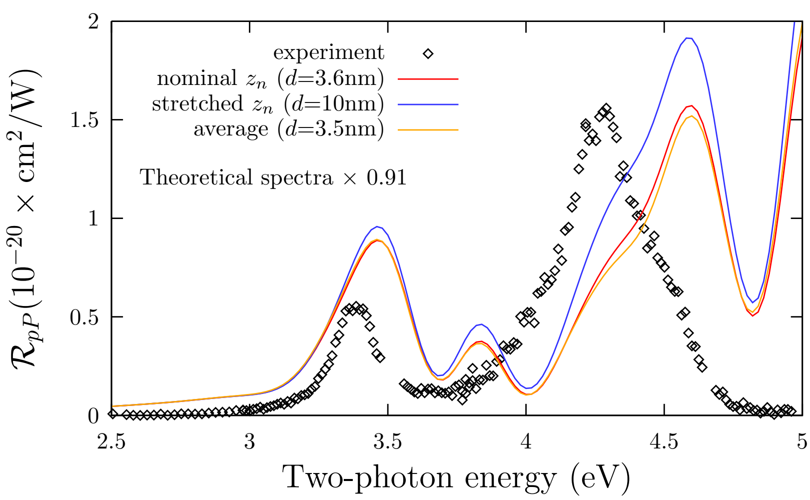

Figure 3. (Color online) $\mathcal{R}_{pP}$ for z_n as given by the slab (nominal, red line), z_n stretched by 2.7 (stretched, blue line), and using the half-slab value of $\chi^{\mathrm{abc}}_{\mathrm{hs}}$ (average, yellow line), see text for details. The experimental data is from Mejía et al. (2002). We use $\theta = 65\,^\circ$, $\phi = 30\,^\circ$, and a broadening of $\sigma = 0.075$ eV.